All in Tokens: Unifying Output Space of Visual Tasks via Soft Token

Jia Ning[1,4*], Chen Li[2,4*], Zheng Zhang[4*], Chunyu Wang[4],
Zigang Geng[3,4], Qi Dai[4], Kun He[1], Han Hu[4]
[1]Huazhong University of Science and Technology
[2]National Key Laboratory of Human-Machine Hybrid Augmented Intelligence,
National Engineering Research Center for Visual Information and Applications,
and Institute of Artificial Intelligence and Robotics, Xi'an Jiaotong University
[3]University of Science and Technology of China [4]Microsoft Research Asia
{ninja, brooklet60}@hust.edu.cn, edward82@stu.xjtu.edu.cn,
{zhez,chnuwa,t-ziganggeng,qid,hanhu}@microsoft.com

Abstract

We introduce AiT, a unified output representation for various vision tasks, which is a crucial step towards general-purpose vision task solvers. Despite the challenges posed by the high-dimensional and task-specific outputs, we showcase the potential of using discrete representation (VQ-VAE) to model the dense outputs of many computer vision tasks as a sequence of discrete tokens. This is inspired by the established ability of VQ-VAE to conserve the structures spanning multiple pixels using few discrete codes. To that end, we present a modified shallower architecture for VQ-VAE that improves efficiency while keeping prediction accuracy. Our approach also incorporates uncertainty into the decoding process by using a soft fusion of the codebook entries, providing a more stable training process, which notably improved prediction accuracy. Our evaluation of AiT on depth estimation and instance segmentation tasks, with both continuous and discrete labels, demonstrates its superiority compared to other unified models. The code and models are available at https://github.com/SwinTransformer/AiT.

1. Introduction

A central goal of AI is to develop a unified model capable of handling many tasks. Recent developments in large-scale language models such as GPT-3 [5] have shown remarkable success as general-purpose solvers for language tasks. It inspires to examine the feasibility of creating universal models for various computer vision tasks.

Current research is approaching the goal from a diverse range of perspectives. Perceiver [18] and Perceiver-IO [17] propose to use exactly the same Transformer architecture to handle different modalities such as natural language, computer vision and StarCraft II. However, it allocates a query for each output and ignores their dependency, making it unable to model interdependent outputs such as the coordinates of a box. Some works attempt to address multiple visual tasks but they are still limited to only a few. For example, Flamingo [1] handles only tasks with language as output; CLIP [31] and its follow-ups [48, 49, 53] tackle only retrieval and image classification tasks; Chen *et al*. [8] deal with tasks that have describable and sequential outputs. Pix2SeqV2 [8] tries to unify different vision tasks using tokens. But the tokens need to be designed manually for each task. For example, they use polygon to represent the instance segmentation, which can not be applied to other tasks such as depth estimation.

In this paper, we aim to develop a comprehensive solution to various vision tasks. To achieve this, we first identify a key challenge in the field - while the NLP tasks typically have similar inputs and outputs represented by language tokens, the outputs of vision tasks are highly diverse. For example, object detection produces labels and coordinates, semantic segmentation generates discrete label maps and depth estimation results in value-rich images. We tackle this hindrance by unifying the output spaces of various visual tasks through a general tokenizer which is implemented using VQ-VAE [36]. It transforms the task output into a set of tokens by the encoder, which are then reconstituted into the original output by the decoder. The task solver for each vision task is realized using an auto-regressive encoder-decoder model. The model takes in images as inputs and outputs a sequence of tokens in a causal manner, which is then converted back into the original task-specific output

*Equal contribution.

using the decoder. we comprehensively assess the impact of various architectural designs in the VQ-VAE model. Our findings reveal that a shallower encoder/decoder architecture, with a maximum of 5 convolution layers, 2 residual blocks, and 128 codebook entries improves inference efficiency without losing prediction accuracy. As a result, the parameters and computations of VQVAE required remain minimal, amounting to only 2 million parameters and 0.06G FLOPs.

To enhance its effectiveness, we propose several innovative techniques that specifically address the unique challenges of visual tasks.

Firstly, we incorporate uncertainty into the decoding process by using a soft fusion of the codebook entries. We represent a soft token by a probability vector where each value representing the probability of membership in the codebook. When a soft token is fed to the detokenizer or the next token prediction network, its input embedding is computed as the weighted average of the corresponding codebook embeddings. This demonstrates that the soft token embedding spans a continuous, interpolable space, which may more accurately reflect visual outputs, particularly in cases where they are continuous in nature. Additionally, the continuous nature of the soft token enables the implementation of an auxiliary loss function, which learns the task output end-to-end.

Secondly, to handle visual tasks that have corrupted, undefined, or invalid values in their annotations, we propose mask augmentation in training. For example, depth estimation is a typical task that faces this challenge, with occluded areas not being defined [35], as shown in Figure 2. These undefined regions can make it difficult for the tokenizer and detokenizer to be trained, as it is not clear what should be reconstructed in these areas. To overcome this issue, we randomly mask segments of the input depth map during VQ-VAE training. Unlike the undefined regions, these manually masked sections have known ground-truth annotations, which help train the VQ-VAE network to be able to recover that ground truth for the undefined regions. Our experiments demonstrate that this technique significantly improves the accuracy.

Thirdly, we propose a Parallel Vision Modeling method on dense vision tokens. Parallel Vision Modeling uses a fixed embedding as the input of the dense token prediction instead of the last predicted token. Obviously, Parallel Vision Modeling can accelerate the auto-regressive prediction by predicting a bunch of visual tokens at a time, we also show they can improve the performance effectively. This method is similar to Perceiver-IO [17] and DETR [6], but unlike the Perceiver-IO which only uses the cross-attention and DETR which uses the bidirectional self-attention, Parallel Vision Modeling uses the unidirectional attention with causal mask and only applied to a portion of tokens, which is more general and can be inserted into any auto-regressive model.

We mainly study our method on two classical visual tasks with diverse outputs: depth estimation and instance segmentation, utilizing floating-point maps and binary masks as output formats. These tasks differ in the size of their output, with depth estimation having a fixed size and instance segmentation having a variable size. Our approach achieved competing results. In particular, it achieves the state-of-the-art results on the NYUv2 depth estimation benchmark [35]. The proposed framework and techniques are versatile, and we also show more results on other tasks in experiment.

2. Related Works

Unified Frameworks in Computer Vision Encouraged by the success of T5 [32]/GPT [5] in NLP, the exploration of a single unified model for various tasks in computer vision has emerged. However, most existing works[1, 48, 49, 38, 53] are focused on the training algorithm or model architectures. This makes these models either only available as pre-trained models [48, 49, 38] or only for VL-related tasks [1, 53]. Perceiver-IO [18] presents a framework that can process different vision tasks, and it adopts the learned positional encoding or Fourier feature to unify the output of different tasks.

Very recently, Pix2SeqV2 [8] proposed to unify different vision tasks into tokens and the tokens in Pix2SeqV2 need to be designed manually for different tasks. For example, they use the polygon to represent the instance segmentation.

The most related works with ours are UViM [20] and Unified-IO [27]. They also adopt VQ-GAN/VQ-VAE as a general tokenizer/detokenizer and an auto-regressive Transformer encoder/decoder to solve different tasks. However, they are direct applications of these techniques without an in-depth consideration of the particularity of visual problems.

Our study, while concurrently started, takes more in-depth consideration of the particularity of visual problems. We propose techniques of soft token and mask augmentation, which prove beneficial generally for visual tasks or a part of them. We also extensively investigate the architecture of the VQ-VAE, which shows that this part can be made very light-weight, and thus make the framework more practical.

Vector-Quantization Discretized token output space is widely used in generative models, such as DALL-E[33], VQGAN[12], and VQ-Diffusion[14], to represent high-dimensional complex data. Models like VQ-VAE[36], dVAE[2] define a discrete latent space with the encoder-decoder architecture and a fixed size of codebook, The input

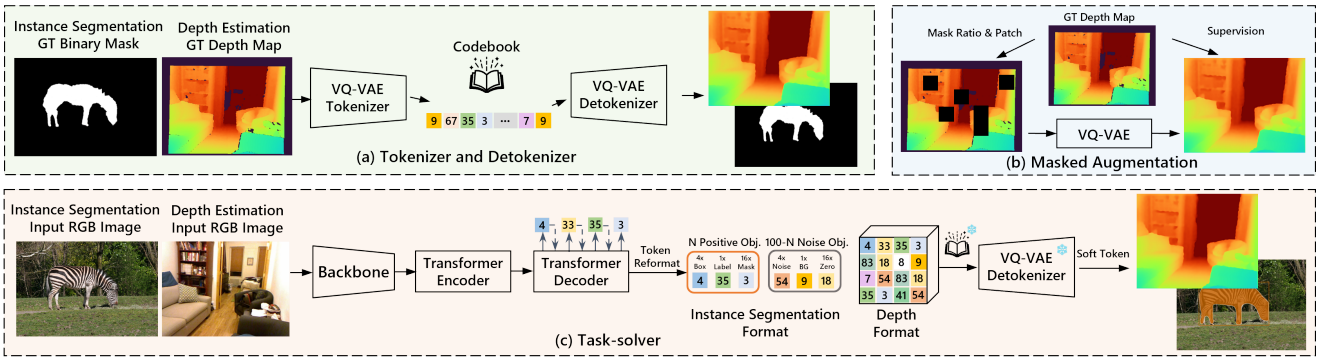

Figure 1. Illustration of our unified framework. (a) VQ-VAE training to learn tokenizer and detokenizer for different tasks. (b) Mask augmentation mitigates the effect when existing corrupted or non-annotated region. (c) In training, various vision task outputs are transferred to discrete token space by a tokenizer. In this way, discrete or continuous visual tasks can be converted into one discrete classified task. In inference, the tokens predicted by the task-solver are decoded by the detokenizer into task outputs. Soft token is applied to improve the token representation

is mapped to the discrete tokens of the codebook. We adopt the VQ-VAE framework to build our token space, and our soft token approach that treats the token space as a continuous one instead of the original discrete one expands the usage of VQ-VAE.

Monocular Depth Estimation Monocular depth estimation is a fundamental task for 3D perception. Deep learning dominates the depth estimation since Eigen *et al*. [11] introduces it into the depth task. The follow-up works include proposing powerful network [22, 34, 23], designing novel augmentation [19, 16], making use of the geometric constraints [30, 47], exploring pairwise relationship [54, 9, 21], combing with conditional random field [25, 44, 50].

Some works [28, 51, 37, 34, 46] combine depth estimation with other tasks, such as semantic segmentation, and edge estimation. However, they design different heads and loss functions for different tasks respectively. There are also some methods [13, 10, 3, 4, 24] discretizing the continuous depth and cast the depth estimation as a per-pixel classification task. Our approach represents the depth maps as a set of tokens, and unifies it with other visual tasks, *i.e*. instance segmentation, in a unified network structure and output space. More importantly, we show that a general framework for various visual tasks can achieve state-of-the-art accuracy on the NYUv2 depth estimation task.

Instance Segmentation Instance segmentation aims to predict the segments of each instance. There are many works [15, 45, 41] studying how to represent the masks. For example, MaskRCNN [15] used a binary mask, Dense RepPoints [45] adopts a set of deformable points to represent the segments, and PolarMask [41] models the segments by polygons. While their representation is specific to instance segmentation, we model the instance segmentation by a set of discrete (soft) tokens, which is more general for visual representations.

3. Framework

The goal of this work is to unify the output space of visual tasks into discrete tokens and to build a single model that can handle different tasks simultaneously. In this section, we present the framework to achieve this goal, which is shown in Figure 1. The framework consists of three modules, a *tokenizer* that encodes the task output to the discrete tokens, a *detokenizer* that decodes tokens to the task output, and a *task-solver* that predicts tokens from images. In our approach, the encoder and decoder of VQ-VAE are used as the tokenizer and detokenizer, and the task-solver is implemented by an auto-regressive encoder-decoder model. During training, task annotations are first mapped by the tokenizer as discrete tokens and used as supervision to train the task-solver. In inference, the tokens predicted by the task-solver are decoded by the detokenizer into task outputs.

3.1. Tokenizer and Detokenizer

VQ-VAE is an encoder-decoder model with a set of latent codes $\mathcal{C}$. It was originally proposed to learn discrete representation for natural images. In this work, we use its encoder E and decoder D as the tokenizer and detokenizer. In training, the input image is encoded as a set of contiguous embeddings, and these embeddings are assigned to their nearest latent codes, we denote this quantization operator as Q. In the decoder, the corresponding codes are used as inputs instead of contiguous embeddings and then decoded into the image. Therefore, the encoder, decoder, and latent codes can be trained by minimizing the reconstruction loss term and commitment loss term:

$$L_{vae} = \|x - D(Q(E(x))\|_2 + \lambda \|E(x) - Q(E(x))\|_2 \quad (1)$$

where x indicates task annotations, λ indicates loss weights.

Since we adopt discrete tokens as targets in the task-solver, the accuracy of reconstruction has an upper-bound on the performance of the whole framework. In addition, both training and inference of task-solver require the tokenizer and detokenizer, the fast inference speed is also desired.

The original network architecture of VQ-VAE is designed for natural images, which have more complex textures and colors than the task output, making it not the optimal design for us. Therefore, we have exhaustively studied the effects of VQ-VAE with different design choices in our framework.

Typical reconstruction losses (*e.g.* l-1 loss, MSE loss, *etc.*) cannot directly reflect the realistic performance of the task, we use standard evaluation metrics for different tasks to measure VQ-VAE. As shown in Table 3 and Table 5. We found that a very lightweight VQ-VAE can achieve promising results in depth estimation and instance segmentation.

In addition, compared to the standard VQ-VAE usually adopts a large codebook size (*e.g.* 8192), our codebook size $|\mathcal{C}|$ can be reduced to 128. We note that though larger $|\mathcal{C}|$ consistently improves VQ-VAE reconstruction ability, they show no difference when applied to task-solver (see Table 2 and Table 3). There are two speculations on the effectiveness of a small codebook: 1) the output space of depth and segmentation is simple, without the need for a large codebook; 2) the large codebook may increase the learning difficulty for task-solver.

There are two speculations on the effectiveness of a small codebook and shallower encoder/decoder: 1) the output space of depth and segmentation is simple, without the need for a large codebook and complex architecture; 2) the large codebook may increase the learning difficulty for task-solver.

3.2. Task-solver

The task-solver is an auto-regressive encoder-decoder network. The encoder is a Swin Transformer with 6 additional standard transformer blocks, each block consists of a self-attention and an FFN. The decoder has 6 blocks, each block consists of a self-attention, a cross-attention, and an FFN. The architecture we used is similar to [7].

Given an input image, the encoder is first applied to learn a generic representation of all tasks. Then, based on the given *task token*, the decoder is used to predict a token sequence in an auto-regressive manner. For different tasks, we customize their sequence formats, as described in the following:

Depth Estimation The task token of depth estimation is denoted as `[DEP]`. It has a straightforward format, which is a token sequence of length $\frac{HW}{32^2}$, where H and W are the height and width of input images, respectively.

Instance Segmentation The sequence format of instance segmentation is more complicated than depth estimation, which consists of three parts: bounding box coordinates, class of bounding box, and a binary mask. We follow the practice of Pix2Seq [7] for representing coordinates and the class of a bounding box. The coordinates are manually quantized into 2000 bins, and different classes are represented by different tokens (including a background class, *e.g.* COCO dataset has 81 class tokens in total). For the binary mask, we use 4×4 tokens to represent one mask. It is worth noting that since the computational complexity of auto-regressive is proportional to the square of the output sequence length, we have to use very few tokens to represent the mask. Nevertheless, benefitting from our powerful detokenizer, these tokens can be decoded to a 64×64 mask. Based on these designs, each instance is represented by a total of 21 tokens (*i.e.* 4 tokens for coordinates, 1 token for class, 16 tokens for mask), and we use `[INS]` as the task token of instance segmentation, as shown in Figure 1 (c). We append the meaningless zero mask for the noise box and do not add loss on those mask tokens during training.

3.3. Soft Token

In a typical auto-regressive prediction procedure, the token with the maximal predicted probability is selected as the output, and used its embedding as the input to the decoder for the next prediction step. This approach is called *hard-inference*, formulated as:

$$\hat{k} = \texttt{argmax}_k P(k|t_0, .., t_{i-1}) \tag{2}$$

$$t_i = \mathcal{C}_{\hat{k}} \tag{3}$$

where t_i indicates i-th predicted token embedding by auto-regressive task-solver model, k is the code index, and $\mathcal{C}_{\hat{k}}$ indicates the embedding of $\hat{k}$-th code in the codebook.

However, since the tokens learned by VQ-VAE are not completely independent of each other, the correlation between the tokens may affect the token prediction accuracy, making the hard inference probably not optimal. To leverage the correlation, a *soft token* technique is presented in the inference: instead of directly using the embedding of a single token, the soft token is the weighted averaged embedding of different tokens by their prediction probability, formulated as:

$$t_i = \sum_{k}^{|\mathcal{C}|} P(k|t_0, .., t_{i-1})\mathcal{C}_k, \tag{4}$$

In addition to being applied in task-solver to predict the next token more accurately, the same idea can also be used in detokenizor to get better reconstruction results.

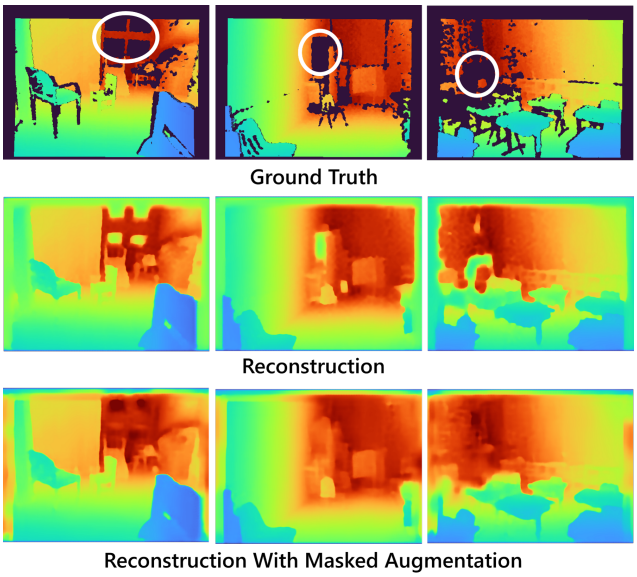

Figure 2. There are some corrupted regions (black regions/pixels) in the GT depth map. While we have ignored these regions in training VQ-VAE as well, the reconstructed regions are still abnormal, which is reflected in the shadows in reconstruction results. This phenomenon can be alleviated by adding masked augmentation.

Furthermore, the soft token results in the embedding space being spanned to an interpolable continuous space. Therefore, we can introduce an auxiliary loss that learns the task-specific output targets in an end-to-end manner by backing from the detokenzior output to the task-solver input.

In Table. 1, we compare the l-2 distance between predicted token embedding and ground-truth token embedding on NYUv2 dataset. We note that the use of soft tokens reduces the distance, indicating that the predicted token embedding is more accurate and also reflect the better RMSE performance. More examinations about soft token in both instance segmentation and depth estimation are shown in ablation study. It can consistently improve the performance without any additional computational cost, which is a *free-lunch* technique in inference.

Table 1. The l-2 distance between predicted token embedding and ground-truth token embedding on NYUv2 dataset.

description.	l-2 dist	RMSE
hard inference	4.78	0.3182
soft token	4.52	0.3080

3.4. Mask Augmentation in Depth Estimation

The ground-truth depth maps in the depth estimation dataset often have some corrupted regions that are not annotated with depth information. In the conventional depth estimation frameworks, these regions are ignored during training. However, the same solution cannot be applied to our framework. There are two challenges: First, while we have ignored these regions in training VQ-VAE as well, the reconstructed regions are still abnormal (see Figure 2) and further affect the training of the task-solver and make the final result also have many artifacts; Second, a token predicted by VQ-VAE corresponds to a 32^2 patch, which may contain both normal and corrupted pixels. Therefore, it is hard to deal with this issue by ignoring the tokens.

As shown in Figure 1 (b), we present to introduce mask augmentation in the training of VQ-VAE to alleviate this challenge. Specifically, we randomly mask some regions in the input depth images and then use their original depth information as supervision. In this way, the VQ-VAE can complete/recover some corrupted regions with reasonable results. Figure 2 shows the visualization. In Table 11, we notice that applying mask augmentation can improve the performance of depth estimation.

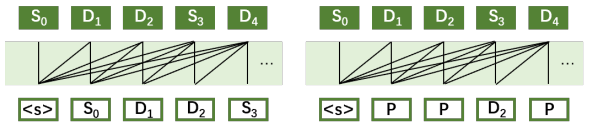

(a) AR modeling with causal attention (b) Parallel modeling with causal attention

Figure 3. The difference between our proposed parallel modeling approach and traditional auto-regressive method. (a) For both sparse token (S) and dense token (D), auto-regressive modeling method using last output token with causal attention to predict next token, leading to a misalignment between training and inference. (b) We use parallel token (P) for dense token prediction, while keeping the causal attention to shrink the gap.

3.5. Parallel Vision Modeling

In traditional auto-regressive models, as shown in Figure 3 (a), at the position i, t_{i-1} is used as the query to predict the token t_i. However, this may cause the information leakage in training, leading to easy training but difficult inference. The misalignment between training and inference can be solved by passing a fixed embedding called parallel token as the query to predict t_i, where t_i is the dense token passed to VQ-VAE decoder afterwards, *e.g.* mask tokens in instance segmentation. We also show in Table 10 and Table 12 that the application of parallel vision modeling can make token prediction more stable and improve the performance significantly.

4. Experiments

4.1. Tasks and Datasets

To examine the generalizability of our framework, we mainly study depth estimation and instance segmentation,

which are two tasks with very different output spaces. We also train the model on more tasks with the same method and attach the results at the end.

Instance Segmentation The instance segmentation requires predicting the location, the class, and the mask of each instance. The COCO2017 benchmark is one of the most challenging datasets for this task. It consists of 117K training images, 5K validation images, and 41K test images. A total of 80 classes annotation are provided. In our experiments, we follow the common setting of previous works [15, 45, 41] that report the performance on the validation set for comparison.

Depth Estimation Depth estimation is a fundamental problem in computer vision, which requires estimating the depth for each pixel. Unlike segmentation whose output is a binary mask, the depth map is a floating point image. In this work, we use the NYUv2 Depth dataset, which consists of 24K training images and 654 validation images, and the RMSE is used as the major metric.

Semantic Segmention Semantic Segmentation need to predict the class and its semantic mask. ADE20K [52] is a widely-used semantic segmentation dataset with 150 semantic classes and 25K images in total, with 20K for training, 2K for validation, and another 3K for testing. mIOU is reported.

Keypoint Detection Keypoint detection is an essential task in computer vision, which focuses on accurately predicting the spatial locations of all human body keypoints within a given image, resulting in a floating-point coordinate vector output format. In our study, we utilize the widely-used COCO keypoint dataset, which comprises 117k training images and an additional 5k validation images. To evaluate the performance of our approach, we employ the Average Precision (AP) based on Object Keypoint Similarity (OKS) as the primary evaluation metric.

4.2. Implementation Details

Since the input value ranges for depth estimation and instance segmentation are different. We train two VQ-VAE models for two tasks separately, and they have similar architecture. For depth estimation, the encoder consists of 5 convolution layers (kernel size is 3 and stride is 2) and follows 2 residual blocks. The output feature map has a downsample ratio of 32, and the channel dimension is progressively increased from 16 to 256. The architecture of the decoder is symmetrical to the encoder, only replacing the convolution layers with the deconvolution layer. For instance segmentation, we reduce the convolution and deconvolution of the encoder and decoder from 5 layers to 4 layers and keep all others the same. Subsequently, the downsample ratio is changed to 16.

In VQ-VAE training, for depth estimation, the input image size used in depth is 480^2, with a batch size of 8. The Adam optimizer is used with the base learning rate of 3e-4, $\beta_1 = 0.9$, $\beta_2 = 0.999$. An exponential learning rate schedule is applied with the learning rate decay of 0.98 and a total of 20 training epochs. For instance segmentation. The input image size is 64^2 with a batch size of 512. The Adam optimizer is used with the base learning rate of 3e-4, $\beta_1 = 0.9$, $\beta_2 = 0.999$. A cosine learning rate schedule is applied with a total of 20 training epochs. By default, the EMA model update technique is used for all VQ-VAE models.

For the task-solver, we adopt the auto-regressive encoder-decoder architecture, which is similar to Pix2Seq[7]. It consists of a backbone, 6 encoder layers, and 6 decoder layers. We use the SwinV2[26] as the backbone, which is pre-trained with SimMIM [43]. Most experiments in the ablation study are separately trained on depth estimation and instance segmentation.

In depth estimation, we use the AdamW optimizer with a base learning rate of 2e-4 and 1e-4, the weight decay of 0.05 and 0.075 for SwinV2-B and SwinV2-L, respectively. The β_1 and β_2 are set to 0.9 and 0.999, and drop path rate is set to 0.1. The total training length is 25 epochs with the batch size of 24. The step learning rate schedule is used and the learning rate dropped to 2e-5 at the 18th epoch. For data augmentation, the random cropping of 480^2 and horizontal flip with probability 0.5 are employed. We also append random brightness contrast, random gamma, and hue saturation value. Auxiliary loss is SILog loss with weight 1.0 for depth estimation.

Training of instance segmentation from scratch is expensive because of the long sequence length. To reduce the cost, we first train an object detection model and then finetuning on instance segmentation. For object detection pretraining, the AdamW optimizer with a base learning rate of 1e-3, a weight decay of 0.05, a drop path rate of 0.3, and a layer decay of 0.85, linear decay learning rate scheduler are applied, and a total of 100 training epochs with a batch size of 128 are performed. For instance segmentation finetuning, we only initialized the backbone and encoder with detection pre-trained model, and randomly initialized the decoder. In addition, AdamW optimizer with a base learning rate of 1e-4, a weight decay of 0.05, and a layer decay of 0.85, linear decay learning rate scheduler are applied, and the total training length is 50 epochs with a batch size of 16. Large-scale jittering with the range of 0.1 to 3.0 and crop size of 640^2 are used for both object detection and instance segmentation. $\beta_1 = 0.9$, $\beta_2 = 0.999$ are used for AdamW in all experiments. Auxiliary loss is DICE loss plus MSE loss with weight 5.0 for instance segmentation.

4.3. Ablation Study

We ablate the key design choices and techniques in this section. By default, we train the model separately for each task in the ablation study for better illustration, and SwinV2-B is used as the default backbone. For depth estimation experiments, a VQ-VAE with codebook size of 128, downsample rate of 32 and mask ratio of 0.5 is used by default. For instance segmentation, the codebook size is 128 and the downsample rate is 16. If not specified, we use the soft token but do not apply auxiliary loss for all ablation experiments.

Table 2. Ablation study on codebook size of VQ-VAE on depth and instance segmentation in reconstruction.

Width	#tokens	Depth	Instance Seg.
		RMSE	Mask mAP
1.0×	64	0.1025	88.94
1.0×	128	0.0966	89.34
1.0×	256	**0.0902**	**90.22**

Table 3. Ablation study on codebook size of VQ-VAE on depth and instance segmentation in task-solver.

Width	#tokens	Depth	Instance Seg.	
		RMSE	Box mAP	Mask mAP
1.0×	64	0.3090	43.5	33.0
1.0×	128	**0.3080**	**43.6**	33.2
1.0×	256	0.3119	43.4	**33.4**

Table 4. Ablation study on the width of VQ-VAE on depth and instance segmentation in reconstruction.

Width	#tokens	Depth	Instance Seg.
		RMSE	Mask mAP
0.5×	128	0.1196	88.97
1.0×	128	**0.0966**	89.34
2.0×	128	0.1025	**90.92**

Table 5. Ablation study on the width of VQ-VAE on depth and instance segmentation in task-solver.

Width	#tokens	Depth	Instance Seg.	
		RMSE	Box mAP	Mask mAP
0.5×	128	0.3127	43.4	33.1
1.0×	128	**0.3080**	**43.6**	**33.2**
2.0×	128	0.3124	43.2	33.1

Architecture of VQ-VAE We study how different designs of VQ-VAE affect performance. We first evaluate the reconstruction performance of different codebook sizes. To more accurately and intuitively observe the reconstruction performance, our evaluation is performed on the validation set of different tasks and adopts mask mAP and RMSE as metrics. The results are shown in Table 2. We find that although the large codebook size (*e.g.* 256) benefits the reconstruction performance, the small codebook size (*e.g.* 64) can also yield sufficiently good reconstruction performance. Further applying to the task-solver, we found different codebook size has little effect on final performance (see Table 3).

Using the same evaluation method, we study the effect of the width of VQ-VAE. Table 4 shows the reconstruction performance and Table 5 shows the performance of applying to task-solver. Similar to the observation on codebook size, we find that the network width has little effect on the final performance. We also study the network depth of VQ-VAE in Table 6, it shows that shallower VQ-VAE can achieve both better efficiency and accuracy.

The downsample ratio of VQ-VAE is another key that may affect network performance. We vary the downsample ratio in [8, 16, 32]. We note that the instance segmentation cannot support a downsample ratio of 8 because it results in too long sequences. Table 7 shows the reconstruction performance, as the downsample ratio increases, the reconstruction performance gets worse, satisfying the intuition. However, we find that better reconstruction performance does not always lead to better performance when applying the VQ-VAE in task-solver. In Table 8, the best performance is achieved at downsample ratio of 32. We explain this phenomenon is that a smaller downsample ratio facilitates reconstruction, but it also increases the length of the token sequence, which is detrimental to the task-solver.

Table 6. Ablation study on increasing the number of residual blocks on the 32× downsampling setting of depth estimation.

#Resblock	Tokenizor	Task-solver
	RMSE	RMSE
2	**0.0966**	**0.3080**
3	0.1055	0.3123
4	0.1082	0.3136
5	0.1033	0.3118

Table 7. Ablation study on the downsample ratio of VQ-VAE on depth and instance segmentation in reconstruction.

Downsample Ratio	Depth	Instance Seg.
	RMSE	Mask mAP
32	0.0966	70.91
16	0.0696	**89.34**
8	**0.0515**	-

Table 8. Ablation study on the downsample ratio of VQ-VAE on depth and instance segmentation in task-solver.

Downsample Ratio	Depth	Instance Seg.	
	RMSE	Box mAP	Mask mAP
32	**0.3080**	42.7	30.3
16	0.3304	**43.6**	**33.2**
8	0.3514	-	-

Table 9. Ablation on the effectiveness of soft token.

Description	Depth	Instance Seg.	
	RMSE	box mAP	mask mAP
Baseline (hard-inf)	0.3174	43.6	31.1
On. task-solver	0.3127	43.5	32.1
On. detokenizor	0.3120	43.6	32.3
On. both	0.3080	43.6	33.2
On. both + aux. loss	**0.3052**	**43.3**	**34.2**

Table 10. Pose estimation, instance segmentation results on COCO val2017 and semantic segmentation on ADE20k validation sets

Method	keypoints(AP)	mask(AP)	ADE20K(mIOU)
SimBa.(SwinV2-B) [39]	76.6	-	-
UperNet(Swin-B) [40]	-	-	48.1
pix2seqv2 [8] O365 pretrain	68.0	37.3	-
Unified-IO$_{XL}$ [27]	68.1(GRIT)	-	-
AiT(SwinV2-B)	67.5	34.2	Unstable
AiT-P(SwinV2-B)	77.4	35.2	50.1

Table 11. Affects of mask augmentation in training VQ-VAE on depth. The patch size of all models is set to 16.

Mask Ratio	VQ-VAE	task-solver
0.0	**0.0831**	0.3105
0.3	0.0893	0.3093
0.5	0.0966	**0.3080**
0.7	0.1196	0.3225

Soft Token To leverage the correlation between tokens, we introduce the soft token techniques, which can be used to improve the performance in the inference stage for free. We examined this technique in Table 9. Compared with the hard inference baseline, applying the soft token in task-solver and detokenzior alone can bring performance gains, and further performance improvement is achieved when used in two stages at the same time: the depth performance is improved by +0.009 RMSE and the instance segmentation is improved by +2.1 mAP. On top of it, adding the auxiliary loss on the output of detokenizor enlarges the gain to +0.012 RMSE and +3.1 mAP.

Mask Augmentation We evaluate the effectiveness of mask augmentation in depth estimation. The different mask ratios vary from 0.3 to 0.7 are used, and Table 11 shows the results. The best performance is achieved by using the mask ratio of 0.5, which is +0.003 better than the baseline. In instance segmentation, it achieves almost the same results as the model without augmentation. This is because segmentation datasets have complete annotations.

4.4. Parallel Vision Modeling

In previous sections, we mainly demonstrate the use of auto-regressive models to unify various visual tasks. In this section, we show the AiT with Parallel Vision Modeling(AiT-P) can help to improve the performance significantly.

Table 12. Results of depth estimation task on NYUv2 [35]. Both AiT and AiT-P are our methods, where AiT indicates auto-regressive prediction, and AiT-P indicates Parallel Vision Modeling.

Method	RMSE ↓	δ_1 ↑	δ_2 ↑	δ_3 ↑	REL ↓	log10 ↓
DORN [13]	0.509	0.828	0.965	0.992	0.115	0.051
BTS [22]	0.392	0.885	0.978	0.995	0.110	0.047
AdaBins [3]	0.364	0.903	0.984	0.997	0.103	0.044
DPT [34]	0.357	0.904	0.988	0.998	0.110	0.045
LocalBins [4]	0.357	0.907	0.987	0.998	0.099	0.042
P3Depth [29]	0.356	0.898	0.981	0.996	0.104	0.043
BinsFormer [24]	0.339	0.921	0.989	0.998	0.096	0.041
NeWCRFs [50]	0.334	0.922	0.992	0.998	0.095	0.041
BinsFormer [24]	0.330	0.925	0.989	0.997	0.094	0.040
SwinV2-B [42]	0.303	0.938	0.992	0.998	0.086	0.037
SwinV2-L [42]	0.287	0.949	0.994	0.999	0.083	0.035
UViM[20]	0.467	-	-	-	-	-
Unified-IO$_{XL}$[27]	0.385	-	-	-	-	-
AiT (SwinV2-B)	0.305	0.934	0.991	0.998	0.087	0.037
AiT (SwinV2-L)	0.284	0.949	0.993	0.999	0.079	0.034
AiT-P (SwinV2-B)	0.301	0.940	0.992	0.998	0.085	0.036
AiT-P (SwinV2-L)	**0.275**	**0.954**	**0.994**	**0.999**	**0.076**	**0.033**
AiT-P (SwinV2-L) w/o soft token	0.282	0.951	0.994	0.999	0.080	0.034

As shown in Table 10 and Table 12, the AiT-P performs better than the pure auto-regressive counterpart along a series of tasks, around 0.01 RMSE (0.275 *vs*. 0.284) on depth, 10 AP gain(77.4 *vs*. 67.5) on COCO keypoints validation and 1 AP(35.2 *vs*. 34.2) gain on COCO instance segmentation. This indicates a strong potential than the pure auto-regressive models. We find the AiT-P has higher loss than AiT because of removing information leakage from training and causes more stable training. Also the parallel prediction can eliminate cumulative error in auto-regressive prediction. With the help of Parallel Vision Modeling, our model can achieve or close the gap with the SOTA task-specific on many tasks.

Our techniques such as *Soft Token* also benefit the parallel decoder, as shown in Table 12. This implies the generality of the proposed techniques.

4.5. Comparison with Other Unified Frameworks and State-of-the-arts in Depth Estimation

UViM and Unified-IO are the most relevant works to ours. We compare the performance with these methods on the overlap task, *i.e*. NYUv2 depth estimation. The results are shown in Table 12. Our auto-regressive approach achieves 0.284 RMSE, which is 0.183 and 0.101 better than UViM and Unified-IO. Moreover, our parallel approach further improves the performance to 0.275 RMSE. This result surpasses previous state-of-the-arts by 0.012 RMSE.

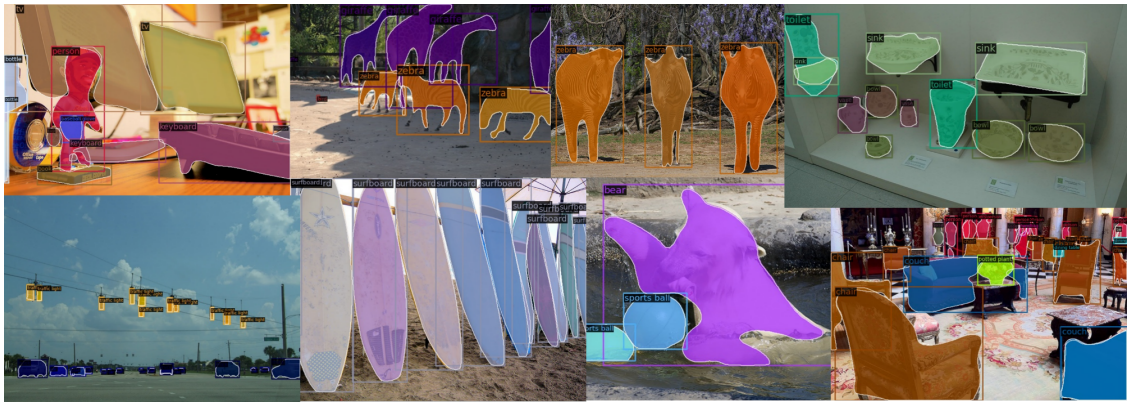

Figure 4. Visualization on instance segmentation task of our methods.

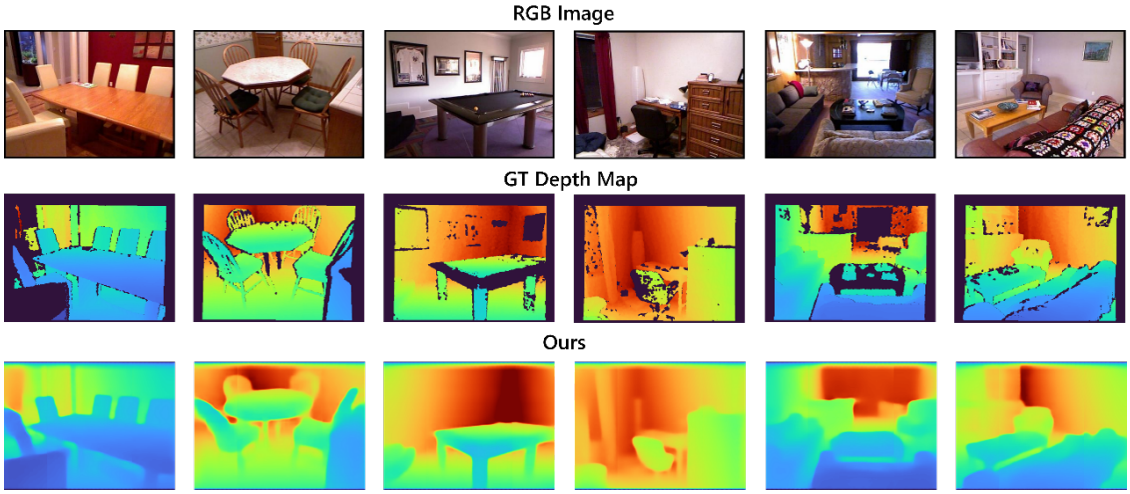

Figure 5. Visualization of depth estimation task of our methods.

While UViM and Unified-IO mainly conceptually propose unified frameworks for various visual tasks, we push more solid steps through in-depth study of the general visual task-solver.

4.6. One Model for Multiple Tasks

We train the instance segmentation and depth jointly using a shared task-solver with AiT model. Table 13 shows that the joint training with shared model weights has marginal performance gradation compared to using separate task solvers.

Table 13. Joint training of depth estimation and instance segmentation using a single task-solver. The performance of joint training is slightly worse than using separate task-solvers for each task.

Description.	Depth	Instance Seg.	
	RMSE	Box mAP	Mask mAP
separate training	**0.3052**	**43.3**	**34.2**
joint training	0.3103	42.2	34.1

5. Conclusion

In this work, we investigate the unification of output spaces for various vision tasks by a set of visual tokens, and further develop a unified auto-regressive encoder-decoder model. Three new techniques are proposed which take the particularity of visual tasks into account to improve the system: 1) Soft token can leverage the correlation between tokens to improve performance in the inference stage and enables end-to-end learning for the final visual targets; 2) Mask augmentation is used to alleviate the issue of corrupted/undefined areas of visual tasks, *e.g.* depth estimation. 3) Parallel Vision Modeling is specific designed for dense vision token only and still remains the auto-regressive capability for sequence generation. With these three techniques, our general method sets a new state-of-the-art on the NYUv2 depth dataset, as well as achieves competitive accuracy on many other tasks. We hope our methods serve as an important step to match the performance of the unified model with that of the best traditional model.

References

[1] Jean-Baptiste Alayrac, Jeff Donahue, Pauline Luc, Antoine Miech, Iain Barr, Yana Hasson, Karel Lenc, Arthur Mensch, Katie Millican, Malcolm Reynolds, et al. Flamingo: a visual language model for few-shot learning. *arXiv preprint arXiv:2204.14198*, 2022. 1, 2

[2] Hangbo Bao, Li Dong, and Furu Wei. Beit: Bert pre-training of image transformers. *arXiv preprint arXiv:2106.08254*, 2021. 2

[3] Shariq Farooq Bhat, Ibraheem Alhashim, and Peter Wonka. Adabins: Depth estimation using adaptive bins. In *CVPR*, pages 4009–4018. Computer Vision Foundation / IEEE, 2021. 3, 8

[4] Shariq Farooq Bhat, Ibraheem Alhashim, and Peter Wonka. Localbins: Improving depth estimation by learning local distributions. In Shai Avidan, Gabriel J. Brostow, Moustapha Cissé, Giovanni Maria Farinella, and Tal Hassner, editors, *ECCV*, volume 13661 of *Lecture Notes in Computer Science*, pages 480–496. Springer, 2022. 3, 8

[5] Tom Brown, Benjamin Mann, Nick Ryder, Melanie Subbiah, Jared D Kaplan, Prafulla Dhariwal, Arvind Neelakantan, Pranav Shyam, Girish Sastry, Amanda Askell, et al. Language models are few-shot learners. *Advances in neural information processing systems*, 33:1877–1901, 2020. 1, 2

[6] Nicolas Carion, Francisco Massa, Gabriel Synnaeve, Nicolas Usunier, Alexander Kirillov, and Sergey Zagoruyko. End-to-end object detection with transformers. In *European conference on computer vision*, pages 213–229. Springer, 2020. 2

[7] Ting Chen, Saurabh Saxena, Lala Li, David J Fleet, and Geoffrey Hinton. Pix2seq: A language modeling framework for object detection. *arXiv preprint arXiv:2109.10852*, 2021. 4, 6

[8] Ting Chen, Saurabh Saxena, Lala Li, Tsung-Yi Lin, David J Fleet, and Geoffrey Hinton. A unified sequence interface for vision tasks. *arXiv preprint arXiv:2206.07669*, 2022. 1, 2, 8

[9] Weifeng Chen, Zhao Fu, Dawei Yang, and Jia Deng. Single-image depth perception in the wild. In Daniel D. Lee, Masashi Sugiyama, Ulrike von Luxburg, Isabelle Guyon, and Roman Garnett, editors, *Neurips*, pages 730–738, 2016. 3

[10] Raul Diaz and Amit Marathe. Soft labels for ordinal regression. In *CVPR*, pages 4738–4747. Computer Vision Foundation / IEEE, 2019. 3

[11] David Eigen, Christian Puhrsch, and Rob Fergus. Depth map prediction from a single image using a multi-scale deep network. In *Neurips*, pages 2366–2374, 2014. 3

[12] Patrick Esser, Robin Rombach, and Bjorn Ommer. Taming transformers for high-resolution image synthesis. In *Proceedings of the IEEE/CVF conference on computer vision and pattern recognition*, pages 12873–12883, 2021. 2

[13] Huan Fu, Mingming Gong, Chaohui Wang, Kayhan Batmanghelich, and Dacheng Tao. Deep ordinal regression network for monocular depth estimation. In *CVPR*, pages 2002–2011. Computer Vision Foundation / IEEE Computer Society, 2018. 3, 8

[14] Shuyang Gu, Dong Chen, Jianmin Bao, Fang Wen, Bo Zhang, Dongdong Chen, Lu Yuan, and Baining Guo. Vector quantized diffusion model for text-to-image synthesis. In *Proceedings of the IEEE/CVF Conference on Computer Vision and Pattern Recognition*, pages 10696–10706, 2022. 2

[15] Kaiming He, Georgia Gkioxari, Piotr Dollár, and Ross Girshick. Mask r-cnn. In *Proceedings of the IEEE international conference on computer vision*, pages 2961–2969, 2017. 3, 6

[16] Yasunori Ishii and Takayoshi Yamashita. Cutdepth: Edge-aware data augmentation in depth estimation. *CoRR*, abs/2107.07684, 2021. 3

[17] Andrew Jaegle, Sebastian Borgeaud, Jean-Baptiste Alayrac, Carl Doersch, Catalin Ionescu, David Ding, Skanda Koppula, Daniel Zoran, Andrew Brock, Evan Shelhamer, et al. Perceiver io: A general architecture for structured inputs & outputs. *arXiv preprint arXiv:2107.14795*, 2021. 1, 2

[18] Andrew Jaegle, Felix Gimeno, Andy Brock, Oriol Vinyals, Andrew Zisserman, and Joao Carreira. Perceiver: General perception with iterative attention. In *International conference on machine learning*, pages 4651–4664. PMLR, 2021. 1, 2

[19] Doyeon Kim, Woonghyun Ga, Pyunghwan Ahn, Donggyu Joo, Sewhan Chun, and Junmo Kim. Global-local path networks for monocular depth estimation with vertical cutdepth. *CoRR*, abs/2201.07436, 2022. 3

[20] Alexander Kolesnikov, André Susano Pinto, Lucas Beyer, Xiaohua Zhai, Jeremiah Harmsen, and Neil Houlsby. Uvim: A unified modeling approach for vision with learned guiding codes. *arXiv preprint arXiv:2205.10337*, 2022. 2, 8

[21] Jaehan Lee and Chang-Su Kim. Monocular depth estimation using relative depth maps. In *CVPR*, pages 9729–9738. Computer Vision Foundation / IEEE, 2019. 3

[22] Jin Han Lee, Myung-Kyu Han, Dong Wook Ko, and Il Hong Suh. From big to small: Multi-scale local planar guidance for monocular depth estimation. *CoRR*, abs/1907.10326, 2019. 3, 8

[23] Zhenyu Li, Zehui Chen, Xianming Liu, and Junjun Jiang. Depthformer: Exploiting long-range correlation and local information for accurate monocular depth estimation. *CoRR*, abs/2203.14211, 2022. 3

[24] Zhenyu Li, Xuyang Wang, Xianming Liu, and Junjun Jiang. Binsformer: Revisiting adaptive bins for monocular depth estimation. *CoRR*, abs/2204.00987, 2022. 3, 8

[25] Fayao Liu, Chunhua Shen, and Guosheng Lin. Deep convolutional neural fields for depth estimation from a single image. In *CVPR*, pages 5162–5170. IEEE Computer Society, 2015. 3

[26] Ze Liu, Han Hu, Yutong Lin, Zhuliang Yao, Zhenda Xie, Yixuan Wei, Jia Ning, Yue Cao, Zheng Zhang, Li Dong, et al. Swin transformer v2: Scaling up capacity and resolution. In *Proceedings of the IEEE/CVF Conference on Computer Vision and Pattern Recognition*, pages 12009–12019, 2022. 6

[27] Jiasen Lu, Christopher Clark, Rowan Zellers, Roozbeh Mottaghi, and Aniruddha Kembhavi. Unified-io: A unified model for vision, language, and multi-modal tasks. *arXiv preprint arXiv:2206.08916*, 2022. 2, 8

[28] Vladimir Nekrasov, Thanuja Dharmasiri, Andrew Spek, Tom Drummond, Chunhua Shen, and Ian D. Reid. Real-time joint

semantic segmentation and depth estimation using asymmetric annotations. In *ICRA*, pages 7101–7107. IEEE, 2019. 3

[29] Vaishakh Patil, Christos Sakaridis, Alexander Liniger, and Luc Van Gool. P3depth: Monocular depth estimation with a piecewise planarity prior. In *CVPR*, pages 1600–1611. IEEE, 2022. 8

[30] Xiaojuan Qi, Renjie Liao, Zhengzhe Liu, Raquel Urtasun, and Jiaya Jia. Geonet: Geometric neural network for joint depth and surface normal estimation. In *CVPR*, pages 283–291. Computer Vision Foundation / IEEE Computer Society, 2018. 3

[31] Alec Radford, Jong Wook Kim, Chris Hallacy, Aditya Ramesh, Gabriel Goh, Sandhini Agarwal, Girish Sastry, Amanda Askell, Pamela Mishkin, Jack Clark, et al. Learning transferable visual models from natural language supervision. In *International Conference on Machine Learning*, pages 8748–8763. PMLR, 2021. 1

[32] Colin Raffel, Noam Shazeer, Adam Roberts, Katherine Lee, Sharan Narang, Michael Matena, Yanqi Zhou, Wei Li, Peter J Liu, et al. Exploring the limits of transfer learning with a unified text-to-text transformer. *J. Mach. Learn. Res.*, 21(140):1–67, 2020. 2

[33] Aditya Ramesh, Prafulla Dhariwal, Alex Nichol, Casey Chu, and Mark Chen. Hierarchical text-conditional image generation with clip latents. *arXiv preprint arXiv:2204.06125*, 2022. 2

[34] René Ranftl, Alexey Bochkovskiy, and Vladlen Koltun. Vision transformers for dense prediction. In *ICCV*, pages 12159–12168. IEEE, 2021. 3, 8

[35] Nathan Silberman, Derek Hoiem, Pushmeet Kohli, and Rob Fergus. Indoor segmentation and support inference from rgbd images. In *Proceedings of the European Conference on Computer Vision*, pages 746–760. Springer, 2012. 2, 8

[36] Aaron Van Den Oord, Oriol Vinyals, et al. Neural discrete representation learning. *Advances in neural information processing systems*, 30, 2017. 1, 2

[37] Lijun Wang, Jianming Zhang, Oliver Wang, Zhe Lin, and Huchuan Lu. Sdc-depth: Semantic divide-and-conquer network for monocular depth estimation. In *CVPR*, pages 538–547. Computer Vision Foundation / IEEE, 2020. 3

[38] Wenhui Wang, Hangbo Bao, Li Dong, Johan Bjorck, Zhiliang Peng, Qiang Liu, Kriti Aggarwal, Owais Khan Mohammed, Saksham Singhal, Subhojit Som, et al. Image as a foreign language: Beit pretraining for all vision and vision-language tasks. *arXiv preprint arXiv:2208.10442*, 2022. 2

[39] Bin Xiao, Haiping Wu, and Yichen Wei. Simple baselines for human pose estimation and tracking. In *Proceedings of the European conference on computer vision (ECCV)*, pages 466–481, 2018. 8

[40] Tete Xiao, Yingcheng Liu, Bolei Zhou, Yuning Jiang, and Jian Sun. Unified perceptual parsing for scene understanding. In *Proceedings of the European conference on computer vision (ECCV)*, pages 418–434, 2018. 8

[41] Enze Xie, Peize Sun, Xiaoge Song, Wenhai Wang, Xuebo Liu, Ding Liang, Chunhua Shen, and Ping Luo. Polarmask: Single shot instance segmentation with polar representation. In *Proceedings of the IEEE/CVF conference on computer vision and pattern recognition*, pages 12193–12202, 2020. 3, 6

[42] Zhenda Xie, Zigang Geng, Jingcheng Hu, Zheng Zhang, Han Hu, and Yue Cao. Revealing the dark secrets of masked image modeling. *arXiv preprint arXiv:2205.13543*, 2022. 8

[43] Zhenda Xie, Zheng Zhang, Yue Cao, Yutong Lin, Jianmin Bao, Zhuliang Yao, Qi Dai, and Han Hu. Simmim: A simple framework for masked image modeling. In *Proceedings of the IEEE/CVF Conference on Computer Vision and Pattern Recognition*, pages 9653–9663, 2022. 6

[44] Dan Xu, Wei Wang, Hao Tang, Hong Liu, Nicu Sebe, and Elisa Ricci. Structured attention guided convolutional neural fields for monocular depth estimation. In *CVPR*, pages 3917–3925. Computer Vision Foundation / IEEE Computer Society, 2018. 3

[45] Ze Yang, Yinghao Xu, Han Xue, Zheng Zhang, Raquel Urtasun, Liwei Wang, Stephen Lin, and Han Hu. Dense reppoints: Representing visual objects with dense point sets. In *European Conference on Computer Vision*, pages 227–244. Springer, 2020. 3, 6

[46] Hanrong Ye and Dan Xu. Inverted pyramid multi-task transformer for dense scene understanding. In *ECCV*, 2022. 3

[47] Wei Yin, Yifan Liu, Chunhua Shen, and Youliang Yan. Enforcing geometric constraints of virtual normal for depth prediction. In *ICCV*, pages 5683–5692. IEEE, 2019. 3

[48] Jiahui Yu, Zirui Wang, Vijay Vasudevan, Legg Yeung, Mojtaba Seyedhosseini, and Yonghui Wu. Coca: Contrastive captioners are image-text foundation models. *arXiv preprint arXiv:2205.01917*, 2022. 1, 2

[49] Lu Yuan, Dongdong Chen, Yi-Ling Chen, Noel Codella, Xiyang Dai, Jianfeng Gao, Houdong Hu, Xuedong Huang, Boxin Li, Chunyuan Li, et al. Florence: A new foundation model for computer vision. *arXiv preprint arXiv:2111.11432*, 2021. 1, 2

[50] Weihao Yuan, Xiaodong Gu, Zuozhuo Dai, Siyu Zhu, and Ping Tan. New crfs: Neural window fully-connected crfs for monocular depth estimation. *CoRR*, abs/2203.01502, 2022. 3, 8

[51] Zhenyu Zhang, Zhen Cui, Chunyan Xu, Yan Yan, Nicu Sebe, and Jian Yang. Pattern-affinitive propagation across depth, surface normal and semantic segmentation. In *CVPR*, pages 4106–4115. Computer Vision Foundation / IEEE, 2019. 3

[52] Bolei Zhou, Hang Zhao, Xavier Puig, Tete Xiao, Sanja Fidler, Adela Barriuso, and Antonio Torralba. Semantic understanding of scenes through the ade20k dataset. *International Journal of Computer Vision*, 127:302–321, 2019. 6

[53] Xizhou Zhu, Jinguo Zhu, Hao Li, Xiaoshi Wu, Hongsheng Li, Xiaohua Wang, and Jifeng Dai. Uni-perceiver: Pre-training unified architecture for generic perception for zero-shot and few-shot tasks. In *Proceedings of the IEEE/CVF Conference on Computer Vision and Pattern Recognition*, pages 16804–16815, 2022. 1, 2

[54] Daniel Zoran, Phillip Isola, Dilip Krishnan, and William T. Freeman. Learning ordinal relationships for mid-level vision. In *ICCV*, pages 388–396. IEEE Computer Society, 2015. 3